Structure and Compressibility of Synthetic ZnAl2O4 (Gahnite) Under High-Pressure Conditions, from Synchrotron X-Ray Powder Diffraction

Article *in* Physics and Chemistry of Minerals · October 2001

DOI: 10.1007/s002690100194

CITATIONS
63

READS
87

4 authors, including:

Davide Levy
Tel Aviv University
64 PUBLICATIONS **1,060** CITATIONS

SEE PROFILE

Vittoria Pischedda
Claude Bernard University Lyon 1
58 PUBLICATIONS **1,155** CITATIONS

SEE PROFILE

Phys Chem Minerals (2001) 28: 612–618

ORIGINAL PAPER

D. Levy · A. Pavese · A. Sani · V. Pischedda

Structure and compressibility of synthetic $ZnAl_2O_4$ (gahnite) under high-pressure conditions, from synchrotron X-ray powder diffraction

Received: 15 January 2001 / Accepted: 23 April 2001

Abstract The structural behavior of synthetic gahnite ($ZnAl_2O_4$) has been investigated by X-ray powder diffraction at high pressure (0–43 GPa) and room temperature, on the ID9 beamline at ESRF. The equation of state of gahnite has been derived using the models of Birch–Murnaghan, Vinet and Poirier–Tarantola, and the results have been mutually compared (the elastic bulk modulus and its derivatives versus P determined by the third-order Birch–Murnaghan equation of state are $K_0 = 201.7(\pm 0.9)$ GPa, $K_0' = 7.62(\pm 0.09)$ and $K_0'' = -0.1022$ GPa^{-1} (implied value). The compressibilities of the tetrahedral and octahedral bond lengths [0.00188(8) and 0.00142(5) GPa^{-1} at $P = 0$, respectively], and the polyhedral volume compressibilities of the four- and sixfold coordination sites [0.0057(2) and 0.0041(2) GPa^{-1} at $P = 0$, respectively] are discussed.

Key words Synthetic-gahnite · EoS · Structural behaviour at HP

D. Levy · V. Pischedda
Dipartimento Scienze Mineralogiche e Petrologiche-
Università degli Studi di Torino,
Via Valperga Caluso 35, 10025 Torino, Italy

A. Pavese (✉)
Dipartimento Scienze della
Terra-Università degli Studi di Milano,
Via Botticelli 23, 20133 Milano, Italy
e-mail: alessandro.pavese@unimi.it
Tel.: +39-02-23698321; Fax: +39-02-70638681

A. Pavese
National Research Council,
Centro di Studio per la Geodinamica Alpina e Quaternaria,
Via Botticelli 23-20133 Milano, Italy

A. Sani
European Synchrotron Radiation Facility,
ESRF-F 38043, Grenoble Cedex, France

Introduction

Spinels have a general chemical formula, AB_2O_4, where, in most cases, A is a divalent and B a trivalent cation. The unit cell contains 32 oxygen atoms in cubic close packing, 16 octahedral sites (M) and 8 tetrahedral sites (T) occupied by the A and B cations. In the "normal" spinel structure, the divalent A atoms fill the T sites and the trivalent B cations enter the M sites; in the "inverse" structure all the A atoms and half the B atoms occupy the octahedral positions, while the other half of the B atoms fill the tetrahedral sites. Intermediate atomic distributions often occur, and are characterized by the degree of inversion, defined as the fraction of B on the T site; temperature triggers cation disordering over the M and T sites (Yamanaka and Takeuchi 1983; Della Giusta et al. 1996; Redfern et al. 1999; and many more). Though most of the research activity upon spinels is devoted to the order-disorder phenomenology, these minerals exhibit also transformations activated by pressure (Liu 1978; Irifune et al. 1991; Yutani et al. 1997; Funamori et al. 1998; Fei et al. 1999; Levy et al. 2000). Given that spinels are often used as model structures, the investigation of their behaviour under high-pressure (HP) conditions is an important aspect of HP crystal chemistry in general. In this light we have undertaken a study on the behavior of synthetic gahnite ($ZnAl_2O_4$) under P, by means of synchrotron high-pressure X-ray powder diffraction; in particular we have investigated the P–V equation of state (EoS) and the structural properties by the Rietveld technique. Note that: (1) no in situ HP study has been found in the literature on $ZnAl_2O_4$; (2) the present investigation complements a previous study on $ZnFe_2O_4$ (Levy et al. 2000), and contributes to achieving a fuller understanding of how the cation replacement (in the present case Al substitutes for Fe) affects the compressional behaviour of spinel phases.

Experimental

Sample

The sample was synthesized by heating for 72 h at 1500 K a quasi-stoichiometric mixture of analytical purity ZnO and Al_2O_3 reagent grades (99% purity; ZnO and Al_2O_3 provided by Carlo Erba Reagenti and Fluka Sigma-Aldrich, respectively) dried at 900 and 1300 K, respectively. A slight excess of zinc oxide was used. The product was then cooled down to 1000 K at a rate of ≈20 K h^{-1}, maintained for 36 h, and finally brought to room temperature at ≈30 K h^{-1}. The sample was treated with dilute nitric acid to dissolve the residual ZnO. X-ray powder diffraction patterns collected by a X'Pert Philips diffractometer proved that no parent phase was observable in the final product. The composition, $Zn_{0.97(1)}Al_{2.02(2)}O_4$, was determined by the atomic absorption technique (2380 Perkin-Elmer Spectrophotometer) using a normalization to four oxygen atoms. The uncertainties between brackets correspond to standard deviations on the basis of 12 8-s absorbance measurements.

Powder diffraction under HP conditions

HP powder diffraction measurements were carried out at ESRF (Grenoble) on the ID9 beamline, using an angle-dispersive setup. High pressure was achieved by means of a Diamond Anvil Cell (DAC) over the range from 0 (for the sake of brevity we set ambient pressure equal to 0 instead of 0.0001 GPa) up to 43 GPa. We performed two sets of measurements: (1) first, we collected patterns up to 8 GPa by a 250-μm diameter cell (diamond anvils with 600-μm diameter culets) and an ethanol–methanol (1:4) solution as a pressure-transmitting medium, in order to have precise control of the increase of pressure in the low-pressure regime; (2) then powder diffraction patterns were recorded from 4 to 43 GPa by a 125-μm diameter cell (diamond anvils with 250-μm diameter culets) and N_2 as a pressure-transmitting medium. The data obtained in the pressure overlap region are fully consistent with each other; here, we use the data from the former set below 4 GPa and from the latter above. In total, we base the present analysis on 29 datasets. The pressure value was determined from the shift of the fluorescence line of ruby, excited by means of an Ar laser source, using the nonlinear hydrostatic pressure scale after Mao et al. (1986). The ruby single crystal was positioned approximately in the centre of the beam. Equilibrium at a given pressure was assumed achieved when P, monitored every 10th minute, did not oscillate more than 0.01 GPa. The uncertainties on P were estimated at about 0.1 GPa, on the basis of the gradient measured by Mao et al. (1986) (≈0.06 kbar μm^{-1} at our highest P values) and of the beam size (≈0.16 μm in radius). The X-ray beam from the U46 undulator was focused vertically with a Pt-coated Si mirror and horizontally with an asymmetrically cut bent Si(111) Laue monochromator to a spot of ≈30 × 30 μm^2. Diffraction images were collected at the wavelength of $\lambda = 0.41535$ Å, calibrated by Si-NBS, and using an MAR345 imaging plate with 100-μm resolution. Recording of data, readout and erasing the imaging plate required about 1–2 min, 5–6 min and 5–6 min, respectively. Sample-to-plate distance was 366.27 mm, resulting in an angular resolution of about 0.04°. The data collected extend up to $\sin(\theta)/\lambda \approx 0.5$. The two-dimensional images were integrated with FIT2D (Hammersley et al. 1996) into one-dimensional diffraction patterns. The GSAS software package (Larson and Von Dreele 1986) was used to carry out Rietveld structure refinements. Pseudo-Voigt profile functions proved to be appropriate to fit the experimental patterns. The Gaussian and Lorentzian components of the FWHM (full width at half maximum) were parametrized as $\sigma^2 = \sigma_0 \tan(\theta)^2$ and as either $\gamma = \gamma_0/\cos(\theta)$ or $\gamma = \gamma_0 \tan(\theta)$ in the low [< 10 GPa] and high [> 10 GPa] pressure domains, respectively; the σ_0 and γ_0 coefficients were refined. Asymmetry was revealed to be negligible, and the background was modelled by means of cosine-function expansions of ten terms. We tried unsuccessfully to account for the contribution of crystalline N_2 to the diffraction patterns by a multiphase profile treatment. However, refinements performed fixing arbitrarily the amount of crystalline N_2 yielded results in agreement within the uncertainties with those obtained without the N_2 contribution.

The full experiment took approximately 4 days; achievement of equilibrium at given P, and slow increasing of load to avoid overshooting were particularly time-demanding. Two points lying more than 3σ out of the smooth trend of a versus P were neglected in our analysis, being considered as affected by some error of measurement [$P = 37.0(1)$ GPa, $a = 7.7889(2)$ Å; $P = 41.1(1)$ GPa, $a = 7.7606(2)$ Å].

Table 1 sets out the results from Rietveld refinements; note that full-profile methods yield the well-known underestimation of the uncertainties on the lattice parameters.

Results

Equation of state

In Fig. 1 the cell edge (a) of gahnite is plotted as a function of pressure. The observed a values have been fitted by a third-order polynomial in P (i.e. $a = \Sigma_{j=0}^{3} c_j P^j$), whose coefficients are: $c_0 = 8.0911$ (3) Å, $c_1 = -1.28$ (1) 10^{-2} Å GPa^{-1}, $c_2 = 1.67$ (7) 10^{-4} Å GPa^{-2}, $c_3 = -1.3$ (1) 10^{-6} Å GPa^{-3}. The use of a fourth-degree expansion would yield a c_4 coefficient less than 3σ significant.

Table 1 Results from structure Rietveld refinements: lattice parameter (Å) and u coordinate of oxygen for gahnite. $R(F^2) = \mathrm{sqrt}[\Sigma |F_0^2 - F_c^2| / \Sigma F_0^2] \times 100$. $R_{wp} = \mathrm{sqrt}[\Sigma (I_0 - I_c)^2 w]$, where w = weighting factor

P (GPa)	a (Å)	u	R (F^2)	R_{wp}
0.	8.09117 (5)	0.2654 (2)	4.3	2.8
0.3 (1)	8.08843 (6)	0.2654 (2)	7.1	3.7
0.6 (1)	8.08318 (7)	0.2658 (2)	7.7	3.1
0.8 (1)	8.07922 (8)	0.2657 (2)	12.1	3.2
1.8 (1)	8.07098 (9)	0.2656 (2)	15.7	3.9
2.2 (1)	8.0629 (1)	0.2655 (2)	14.6	3.4
3.1 (1)	8.0532 (1)	0.2653 (2)	8.1	3.3
4.6 (1)	8.03340 (8)	0.2654 (2)	3.6	2.7
6.1 (1)	8.01869 (5)	0.2654 (2)	2.5	1.6
8.3 (1)	7.99606 (6)	0.2655 (2)	2.9	1.6
10.8 (1)	7.97037 (6)	0.2653 (2)	3.6	1.6
12.4 (1)	7.95609 (6)	0.2651 (2)	9.0	1.6
13.7 (1)	7.94532 (6)	0.2647 (2)	11.2	1.6
14.5 (1)	7.93640 (7)	0.2647 (2)	9.0	1.6
15.9 (1)	7.92472 (7)	0.2647 (2)	2.2	1.7
16.7 (1)	7.91769 (9)	0.2649 (2)	2.4	2.1
17.7 (1)	7.9090 (1)	0.2651 (3)	4.9	2.5
18.6 (1)	7.9035 (1)	0.2657 (3)	5.4	2.1
19.9 (1)	7.8909 (1)	0.2652 (3)	3.5	2.0
21.0 (1)	7.8837 (1)	0.2647 (3)	2.5	2.0
21.9 (1)	7.8769 (1)	0.2643 (3)	2.8	1.9
23.8 (1)	7.8629 (1)	0.2640 (3)	3.2	1.7
25.4 (1)	7.8523 (1)	0.2640 (3)	2.4	1.7
27.2 (1)	7.8389 (1)	0.2640 (3)	1.6	1.9
29.8 (1)	7.8231 (1)	0.2643 (3)	1.7	1.9
32.2 (1)	7.8083 (1)	0.2643 (3)	2.3	1.8
35.2 (1)	7.7900 (2)	0.2642 (3)	2.3	1.7
39.8 (1)	7.7620 (2)	0.2641 (3)	3.4	1.6
42.9 (1)	7.7452 (2)	0.2639 (3)	3.1	1.2

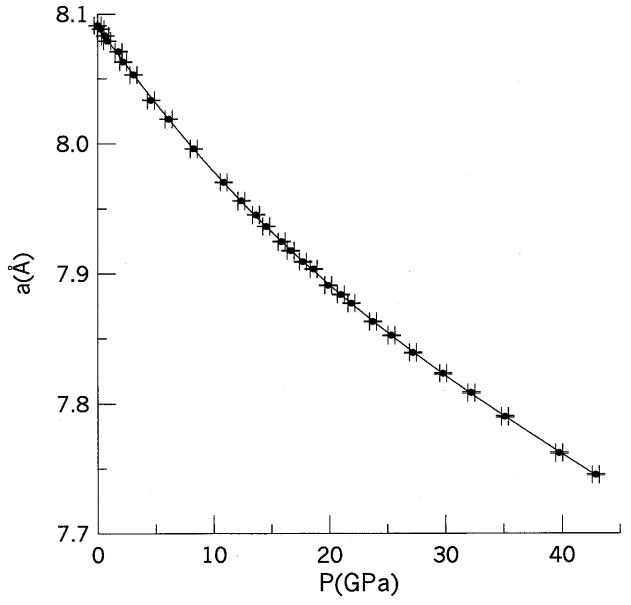

Fig. 1 Cell edge (Å) as a function of pressure (GPa). The *full line* is the third-order polynomial fit. *Error bars* correspond to 3σ

Three models of EoS have been fitted to the present P–V data, in order to have a cross-check on the elastic properties inferred:

1. The Birch–Murnaghan model (Birch 1986), which calculates pressure as

$$P(V) = 3K_0 f_E(1+2f_E)^{5/2}\left(1 + Af_E + Bf_E^2\right) \ , \qquad (1)$$

where K_0 is the bulk modulus at $P = 0$, $A = 3/2(K_0' - 4)$ and $B = 3/2[K_0K_0'' + (K_0' - 4)(K_0' - 3) + 35/9]$, with K_0' and K_0'' corresponding to the first and second derivative of K versus P, at ambient conditions; f_E is the Eulerian strain defined as follows

$$f_E = [(V_0/V)^{2/3} - 1]/2 \ , \qquad (2)$$

where V_0 and V stand for the volume at $P = 0$ and at a given pressure, respectively;

2. The Vinet EoS (Vinet et al. 1986, 1987), expressed through the following equation

$$P(V) = 3K_0 \frac{(1 - f_V)}{f_V^2} \exp[\eta(1 - f_V)] \ , \qquad (3)$$

where $\eta = 3/2(K_0' - 1)$ and $f_V = \left(\frac{V}{V_0}\right)^{1/3}$;

3. The Poirier–Tarantola EoS (Poirier and Tarantola 1998), resulting in

$$P(V) = 3K_0\left(\frac{V_0}{V}\right) f_N\left(1 + Af_N + Bf_N^2\right) \ , \qquad (4)$$

where $A = 3/2(K_0' - 2)$, $B = 3/2[1 + K_0K_0'' + (K_0' - 2) + (K_0' - 2)^2]$ and f_N is the natural strain defined according to

$$f_N = \frac{1}{3}\ln\left(\frac{V_0}{V}\right) \ .$$

The appropriate truncations of Eqs. (1) and (4) have been visually determined by Fig. 2a, b, in which the normalized pressures, defined as $P_{\rm bm} = P/3f_E(1+2f_E)^{5/2}$ and $P_{\rm pt} = P(V/V_0)/3f_N$, are plotted versus f_E and f_N, respectively. Both normalized pressures exhibit linear trends, that naturally suggest choosing third-order truncations, i.e. B coefficients set equal to 0 in Eqs. (1) and (4). Had we used fourth-order expansions for the Birch–Murnaghan and Poirier–Tarantola models, we would have obtained K_0'' values about 1σ significant, and a marked increase of the ESDs of the bulk modulus and of its first derivative versus P.

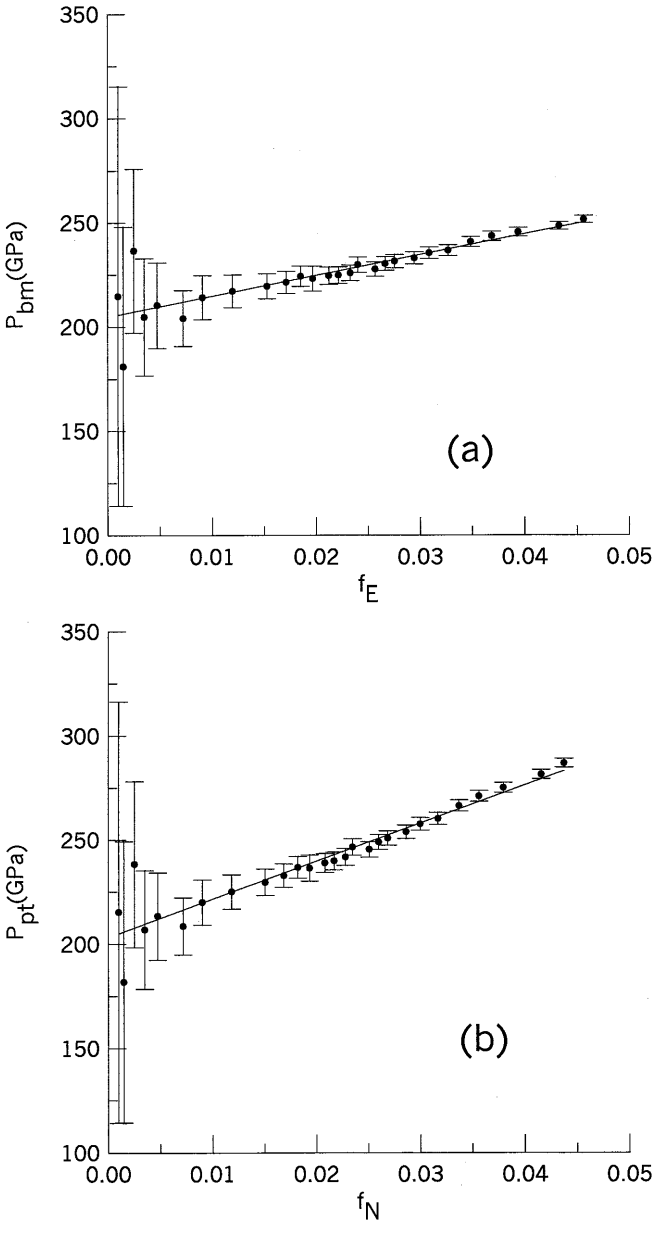

Fig. 2a, b Normalized pressures $P_{\rm bm} = P/3f_E(1+2f_E)^{5/2}$ (**a**) and $P_{\rm pt} = P(V/V_0)/f_N$ (**b**), defined in the text, versus strain. *Error bars* correspond to 3σ

In Table 2 the results achieved by the EoSs reported above are presented; the acronyms used in the discussion below are explained in the caption of Table 2. The

Table 2 Bulk modulus (GPa), its first and second (GPa^{-1}) derivatives versus pressure and the volume at room conditions are set out, according to the Birch–Murnaghan, the Vinet, and Poirier–Tarantola EoSs. *BM3* third-order Birch–Murnaghan EoS; *BM3v* third-order Birch–Murnaghan EoS with refined V_0; *V* Vinet model; *Vv* Vinet model with refined V_0; *PT3* third-order Poirier–Tarantola EoS; *PT3v* third-order Poirier–Tarantola EoS with refined V_0. χ^2 = sqrt[$\Sigma(P_{obs} - P_{calc})^2/\sigma_t^2$]/($N$–$M$), where N = number of pressure measurements, M = degrees of freedom, σ_t = sqrt[$\sigma(P)^2 + (\partial P/\partial V)^2\sigma(V)^2$]

	K_0(GPa)	K_0'	K_0''(GPa^{-1})	V_0($Å^3$)	χ^2
BM3	201.7 (±0.9)	7.62 (±0.09)	−0.1022	529.705	1.09
BM3v	200.4 (±1.7)	7.71 (±0.11)	−0.1065	529.8 (1)	1.09
V	202.2 (±0.8)	7.50 (±0.08)		529.705	1.08
Vv	201.2 (±1.5)	7.55 (±0.11)		529.8 (1)	1.09
PT3	196.6 (±1.1)	8.97 (±0.12)	−0.2876	529.705	1.36
PT3v	193.4 (±2.1)	9.24 (±0.16)	−0.3140	529.9 (1)	1.24

Birch–Murnaghan and Vinet EoSs show similar χ^2 values which, therefore, do not allow for unambiguous choice between models; the Poirier–Tarantola EoS, instead, yields larger χ^2s. We now shift our attention to the consistency between the elastic parameters provided by different EoSs.

BM3, BM3v, V, and Vv give K_0 values deviating from one another by less than 1–2σ. The bulk modulus determined by these models is just slightly sensitive to the refinement of V_0, whose value differs by 1σ from the unrefined one. This demonstrates the full internal consistency of our data, and shows the ability of the Birch–Murnaghan and Vinet EoSs to fit the present P–V data. The Poirier–Tarantola model gives K_0 values in partial disagreement with those provided by the other EoSs, with discrepancies of about 4–5σ; the K_0s issued by PT3 and PT3v differ from one another [≈3 GPa] more than those yielded by BM3 and BM3v [≈1 GPa], and by V and Vv [≈1 GPa].

Likewise, the K_0' values from the Birch–Murnaghan and from the Vinet models are fully consistent within the experimental uncertainties (discrepancies about 1–2σ), and the result is stable upon refining V_0. The Poirier–Tarantola model provides K_0' values larger than those from the other EoSs, and slightly less stable if V_0 is varied.

A way to compare and assess elastic parameters attained by different EoS models consists in using the confidence ellipses (Bass et al. 1981), which take into account the correlations between K_0 and K_0'. In Fig. 3 we plot the confidence ellipses of BM3, for the 68.3, 90 and 99.7% confidence levels. The V model gives K_0 and K_0' values that lie between the 90 and 99.7% confidence ellipses of BM3, while PT3 yields results not consistent with the other two EoSs. In general, the Birch–Murnaghan EoS and the Vinet EoS seem to be more consistent to treat the present data.

If one calculates the bulk modulus at $P = 0$ as the inverse of the volume compressibility, which can readily be obtained by the expansion $a(P)$ given above, K_0 proves to be 211 (±2) GPa. The discrepancy with the issues of the EoSs is presumably ascribable to the partial lack of physics of the plain polynomial expansion in P.

Levy et al. (2000) measured K_0 and K_0' equal to 166 GPa and 9.3, respectively, for synthetic $ZnFe_2O_4$.

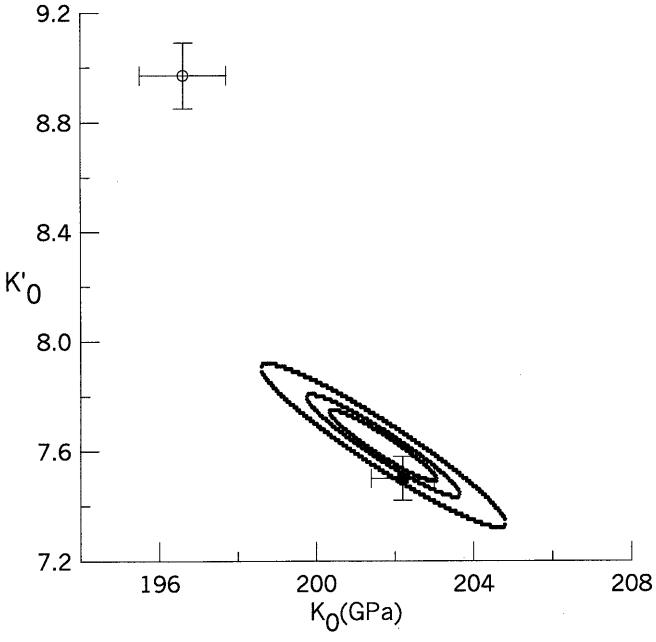

Fig. 3 Confidence ellipses of BM3 at the 68.3, 90 and 99.7% levels of confidence, from *the inner to the outer curve*, respectively. The results of the V model are indicated by a *filled square*, those of the PT3 model by an *open circle*

The significant decrease in compressibility testified by the more than 15% larger bulk modulus of gahnite seems attributable to the replacement of Fe with Al in the octahedral sites, which constitutes the only apparent difference between $ZnAl_2O_4$ and $ZnFe_2O_4$. This point is rediscussed below in the light of the compressibility of the Al octahedron.

Structure versus pressure

The Rietveld structure refinements of gahnite have been carried out assuming a stoichiometric composition, and a fully normal structure because: (1) a refinement at ambient conditions and outside the high-pressure cell has given indications in favor of a slight degree of inversion (0.02 ± 0.05 aluminum per T site) though we have not been able to fix it precisely. This result, in turn,

might be reflective of the non-stoichiometry of the sample; (2) the effects due to a degree of inversion which, if any, is expected to be small (O'Neill and Dollase 1994), would be swamped by the aberrations and uncertainties occurring in measurements under high-pressure conditions.

In Fig. 4 the position coordinate of oxygen (u,u,u) is reported versus P. All the u values lie within an interval less than 3σ wide; the large uncertainties on u are a consequence of the combination of some hindering effects common in HP powder diffraction measurements such as peak broadening, N_2 crystallization, and consequent deviatoric stress. Relying upon the trend only because, in principle, one could not discriminate between the u's observed at different pressures, a linear fit versus P seems to be the least committal function to model a smooth dependence of u on pressure. A weighted linear fit on the u values in Table 1 [$u(P) = u_0 + u_1 P$] gives $u_0 = 0.26559$ (7) and $u_1 = -4.3$ (4) 10^{-5} GPa^{-1}.

In Fig. 5a and b the tetrahedral and octahedral bond lengths are plotted versus pressure. Note the ripple at about 20 GPa exhibited by both T–O and M–O; we have no apparent proof that it is connected with a structural transformation, and hence we assume it just reflects statistical oscillations by which u is affected. This aspect will be rediscussed farther.

The behaviour of an interatomic distance or polyhedral volume in a spinel-like structure is fully determined by a and u. In particular, it is straightforward to prove that any X–Y bond compressibility (β^{X-Y}), or polyhedral volume compressibility (β^{T}or β^{M}, in the case of tetrahedron or octahedron, respectively), can be split into two contributions, i.e.,

$$\beta^{XY} = \beta^{a} + \beta_u^{XY} \tag{5}$$

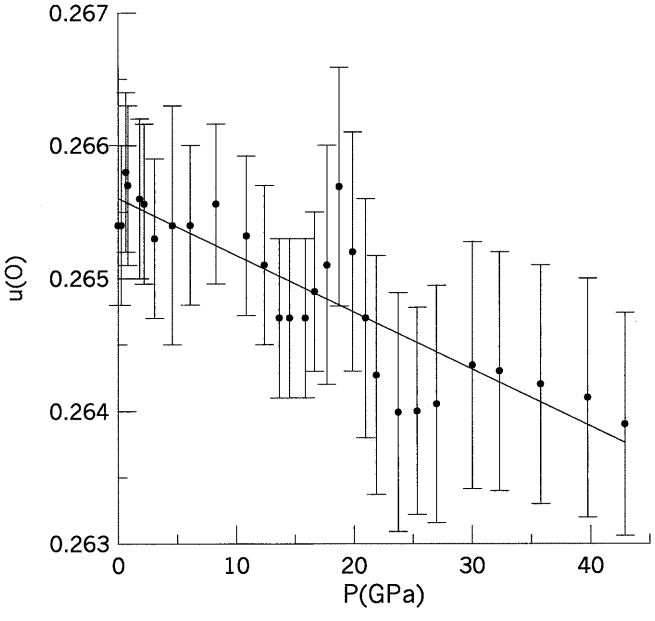

Fig. 4 u as a function of pressure (GPa). *Error bars* correspond to 1σ

$$\beta^{T,M} = \beta + \beta_u^{T,M} \ , \tag{6}$$

where β^{a} is the lattice parameter compressibility, β the cell-volume compressibility ($\beta = 3\beta^{a}$) and β_u^{XY}s are functions of u only. β^{a} and β are henceforth called lattice contributions while β_u^{XY} is addressed as u contribution to the compressibility of a structural observable. Nakagiri et al. (1986) list in detail the formulas which give bond lengths, polyhedral volumes, and compressibilities as a function of a and u.

In Fig. 6 the compressibility of the T–O and M–O bond lengths as a function of P is displayed split after

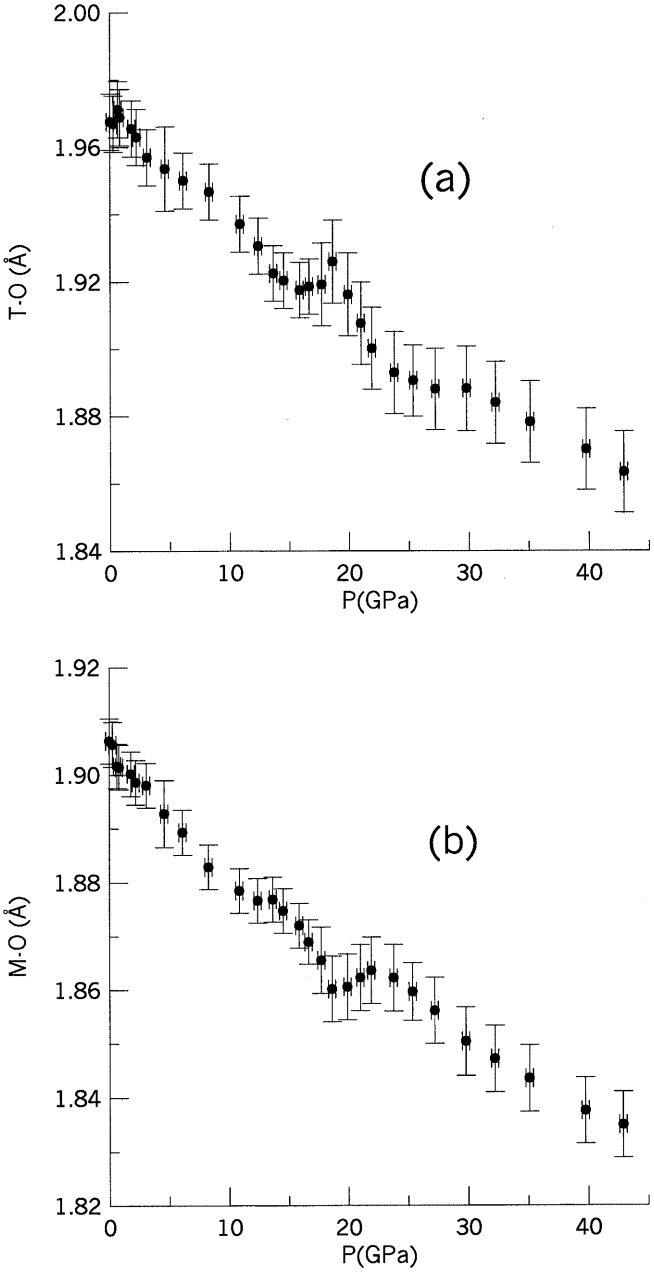

Fig. 5a, b Tetrahedral (**a**) and octahedral (**b**) cation-oxygen bond lengths (Å) reported as a function of pressure (GPa). *Error bars* correspond to 3σ

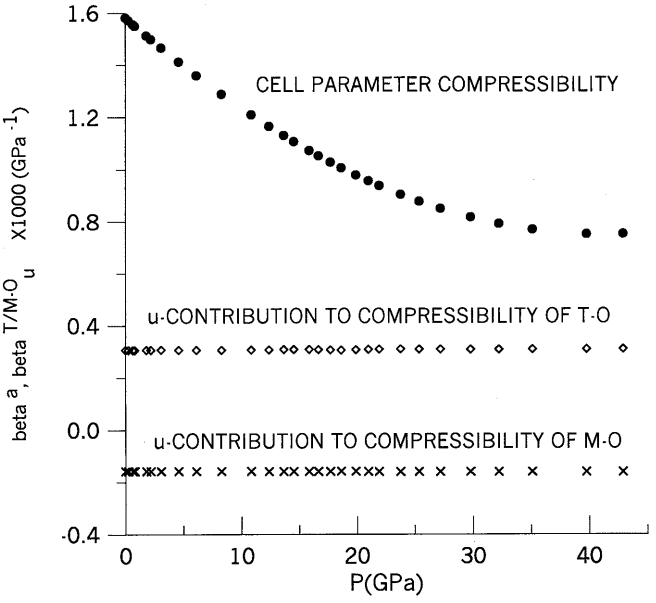

Fig. 6 Contributions to the compressibility of T–O and M–O bond lengths as a function of pressure (GPa). β^{a} (*filled circles*), β_u^{T-O} (*empty diamonds*) and β_u^{M-O} (*crosses*) (GPa^{-1}) are defined in the text (Eq. 5)

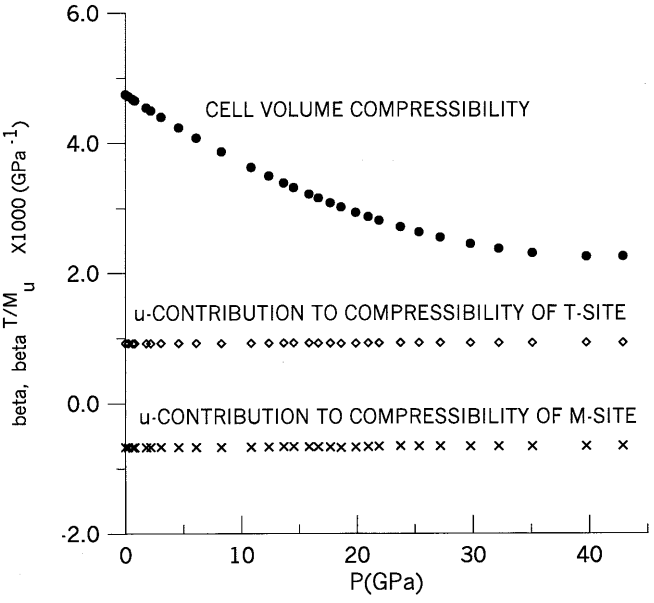

Fig. 7 Contributions to the volume compressibility of tetrahedral and octahedral sites as a function of pressure (GPa). β (*filled circles*), β_u^{T} (*empty diamonds*) and β_u^{M} (*crosses*) (GPa^{-1}) are defined in the text (Eq. 6)

Eq. (5). It is apparent that the lattice contribution dominates the cation-oxygen interatomic distance compressibility, and controls the dependence of β^{T-O} and β^{M-O} on pressure. The u contributions to the tetrahedral and octahedral bond length compressibilities are nearly constant throughout the baric range explored, and are reflective of the modest changes that u undergoes upon P (see Table 1). It is worth observing that $\beta_u^{MO} < 0$ and $\beta_u^{TO} > 0$, which means that M–O would expand while T–O would shorten if the lattice contribution were neglected. This is explainable on crystallographic grounds taking into account that the structure of spinels is dependent on one positional degree of freedom only, whose change inevitably implies either shortening of T–O and lengthening of M–O, or vice-versa. Such a mechanism may also account, intuitively, for the small changes of u upon P in gahnite, which persists at HP: large variations of the coordinate of O under pressure would cause exaggerated shrinking of one site (M or T) with respect to the other (T or M), most likely leading to instability under compression.

In Fig. 7 we plot the tetrahedral and octahedral volume compressibilities partitioned into the lattice and u contributions. Considerations similar to those for the cation-oxygen bond lengths hold for β^{T} and β^{M} as well. $\beta^{T} > \beta^{M}$ is physically due to the fact that the polyhedral compressibility is inversely proportional to the valence of the cation (Hazen and Finger 1982), and in the present case Zn^{2+} enters the T sites, while Al^{3+} occupies the octahedral position.

At $P = 0$ we calculate $\beta^{M-O} = 0.00142$ (5), $\beta^{T-O} = 0.00188$ (8), $\beta^{T} = 0.0057$ (2), and $\beta^{M} = 0.0041$ (2) GPa^{-1}. Finger et al. (1986), in the case of $MgAl_2O_4$, give polyhedral compressibilities equal to 0.0038 (6) and 0.008 (1) GPa^{-1} for octahedron (Al) and tetrahedron (Mg), respectively. By comparing the present issues with those of the quoted authors, β^{M} seems to be weakly sensitive to the chemical species dwelling on the T site, although the replacement between Zn and Mg shifts significantly the elastic features of the tetrahedron, as expected. Nakagiri et al. (1986) measured a compressibility of 0.054 (20) GPa^{-1} for the M site filled by Fe; this value is larger than our β^{M}, and contributes to the explanation of the difference in bulk modulus between gahnite and franklinite mentioned in the previous section.

Lastly, it is noteworthy that Levy et al. (2000) observed franklinite to undergo a phase transition above 22 GPa, whilst gahnite shows no evidence of any transformation activated by pressure (up to 43 GPa), save the ripple at about 20 GPa apparent in Figs. 4 and 5a and b. Note that: (1) no additional peaks are observed in the patterns at higher pressure (which would be expected as most spinels investigated in terms of transformation triggered by P shift to an orthorombic structure: see references in the Introduction); (2) no anomalous increase in the peak widths was revealed; and (3) the spinel structure model satisfactorily holds in terms of structural refinements. The observed stability of the spinel structure to higher pressure might be due either to the replacement of Fe with Al or to a significantly slower reaction kinetics than in franklinite, so that we have not been able to detect any transformation during the experiment, and the ripple at 20 GPa is only a hint of its onset. Alternatively, refinements of the inversion parameter did not give results precise enough to sustain a cation rearrangement triggered by pressure, providing issues less than 1σ significant.

Conclusions

The following conclusions can be drawn from the present high-pressure [0–43 GPa] investigation on synthetic gahnite:

1. The elastic parameters result $K_0 = 201.7$ (± 0.9) GPa, $K_0' = 7.62$ (± 0.09) and $K_0'' = -0.1022$ GPa^{-1}, fitting the observed P–V values by the third-order Birch–Murnaghan EoS; the Vinet EoS confirms these issues, while the Poirier–Tarantola logarithmic EoS yields $K_0 = 196.6$ (± 1.1) GPa, $K_0' = 8.97$ (± 0.12) and $K_0'' = -0.2876$ GPa^{-1}, but with larger χ^2.

2. The bond length compressibilities and the polyhedral volume compressibilities are mainly controlled by the effects of cell-edge shortening, and at $P = 0$ we have obtained $\beta^{M-O} = 0.00142$ (5), $\beta^{T-O} = 0.00188$ (8), $\beta^{T} = 0.0057$ (2), and $\beta^{M} = 0.0041$ (2) GPa^{-1}.

3. At variance with franklinite, gahnite does not show evidence of any phase transition to 43 GPa and room temperature, save a possible ripple at about 20 GPa apparent in the u versus P and T–O versus P curves. Presently we are not able to attribute the persistence of gahnite upon P either to a better pressure stability of $ZnAl_2O_4$ compared to $ZnFe_2O_4$, or to a slow reaction kinetics which prevents us from observing the occurrence of the transformation by in situ high-pressure experiments at room temperature. The possibility of cation reordering as a function of pressure cannot be reliably explored with the present quality of data.

Acknowledgements The authors are grateful to I.Di Gorga for technical support in performing chemical analyses. A.P. is indebted to A. Della Giusta and P.F. Zanazzi for careful review of the manuscript before submission, and to R. Skàla and an anonymous referee for suggestions that really improved the manuscript. This work has been funded by MURST (project Relationships Between Structure and Properties in Minerals: Analysis and Applications) and CNR (Centro di Studio per la Geodinamica Alpina e Quaternaria, Milano). The European Synchrotron Radiation Facility is kindly acknowledged.

References

Bass JD, Liebermann RC, Weidner DJ, Finch SJ (1981) Elastic properties from acoustic and volume compression experiments. Phys Earth Planet Int 25: 140–158

Birch F (1986) Equation of state and thermodynamic parameters on NaCl to 300 kbar in the high temperature domain. J Geophys Res 91: 4949–4954

Della Giusta A, Carbonin S, Ottonello G (1996) Temperature-dependent disorder in a natural Mg–Al–Fe^{2+}–Fe^{3+} spinel. Mineral Mag 60: 603–616

Fei Y, Frost DJ, Mao HK, Prewitt CT, Häusermann D (1999) In situ structure determination of the high pressure phase of Fe_3O_4. Am Mineral 84: 203–206

Finger LW, Hazen RM, Hofmeister AM (1986) High-pressure crystal chemistry of spinel ($MgAl_2O_4$) and magnetite (Fe_3O_4): comparison with silicate spinels. Phys Chem Miner 13: 215–220

Funamori N, Jeanloz R, Nguyen H, Kavner A, Cadwell WA, Fujino K, Miyajima N, Shinmei T, Tomioka N (1998) High-pressure transformations in $MgAl_2O_4$. J Geophys Res 103: 20 813–20 818

Hammersley AP, Svensson SO, Hanfland M, Fitch AN, Häusermann D (1996) Two-dimensional detector software: from real detector to idealised image or two-theta scan. High Press Res 14: 235–248

Hazen RM, Finger LW (1982) Comparative crystal chemistry. Wiley, New York

Irifune T, Fujino K, Ohtuni E (1991) A new high-pressure form of $MgAl_2O_4$. Nature 349: 409–411

Larson AC, Von Dreele RB (1986) GSAS: general structure analysis system. Los Alamos National Laboratory, Report LAUR: 86–87

Levy D, Pavese A, Hanfland M (2000) Phase transition of synthetic zinc ferrite spinel ($ZnFe_2O_4$) at high pressure, from synchrotron X-ray powder diffraction. Phys Chem Miner 27: 638–644

Liu LG (1978) A new high-pressure phase of spinel. Earth Plan Sci Lett 41: 398–404

Mao HK, Xu J, Bell PM (1986) Calibration of the ruby pressure gauge to 800 kbar under quasi-hydrostatic conditions. J Geophys Res 91: 4673–4676

Nakagiri N, Manghnani MH, Ming LC, Kimura S (1986) Crystal structure of magnetite under pressure. Phys Chem Miner 13: 238–244

O'Neill HStC, Dollase WA (1994) Crystal structures and cation distributions in simple spinels from powder XRD structural refinements: $MgCr_2O_4$, $ZnCr_2O_4$, Fe_3O_4 and the temperature dependence of the cation distribution in $ZnAl_2O_4$. Phys Chem Miner 20: 541–555

Poirier JP, Tarantola A (1998) A logarithmic equation of state. Phys Earth Planet Int 109: 1–8

Redfern SAT, Harison RJ, O'Neill StCH, Wood DRR (1999) Thermodynamic and kinetics of cation ordering in $MgAl_2O_4$ synthetic spinel up to 1600° from in situ neutron diffraction. Am Mineral 84: 299–310

Vinet P, Ferrante J, Smith JR, Rose JH (1986) A universal equation of state for solids. J Phys (C): Solid State 19: L467–L473

Vinet P, Smith JR, Ferrante J, Rose JH (1987) Temperature effects on the universal equation of state of solids. Phys Rev (B) 35: 1945–1953

Yamanaka T, Takeuchi Y (1983) Order-disorder transition in $MgAl_2O_4$ spinel at high temperatures up to 1700 °C. Z Kristallogr 165: 65–78

Yutani M, Yagi T, Yusa H, Irifune T (1997) Compressibility of calcium ferrite-type $MgAl_2O_4$. Phys Chem Miner 24: 340–344